

# SHOCK WAVES IN DISPERSIVE HYDRODYNAMICS WITH NON-CONVEX DISPERSION

PATRICK SPRENGER, MARK A. HOEFER

*Department of Applied Mathematics, University of Colorado, Boulder, Colorado 80309-0526, USA*

**ABSTRACT.** Dissipationless hydrodynamics regularized by dispersion describe a number of physical media including water waves, nonlinear optics, and Bose-Einstein condensates. As in the classical theory of hyperbolic equations where a non-convex flux leads to non-classical solution structures, a non-convex linear dispersion relation provides an intriguing dispersive hydrodynamic analogue. Here, the fifth order Korteweg-de Vries (KdV) equation, also known as the Kawahara equation, a classical model for shallow water waves, is shown to be a universal model of Eulerian hydrodynamics with higher order dispersive effects. Utilizing asymptotic methods and numerical computations, this work classifies the long-time behavior of solutions for step-like initial data. For convex dispersion, the result is a dispersive shock wave (DSW), qualitatively and quantitatively bearing close resemblance to the KdV DSW. For non-convex dispersion, three distinct dynamic regimes are observed. For small amplitude jumps, a perturbed KdV DSW with positive polarity and orientation is generated, accompanied by small amplitude radiation from an embedded solitary wave leading edge, termed a radiating DSW or RDSW. For moderate jumps, a crossover regime is observed with waves propagating forward and backward from the sharp transition region. For jumps exceeding a critical threshold, a new type of DSW is observed we term a translating DSW or TDSW. The TDSW consists of a traveling wave that connects a partial, non-monotonic, negative solitary wave at the trailing edge to an interior nonlinear periodic wave. Its speed, a generalized Rankine-Hugoniot jump condition, is determined by the far-field structure of the traveling wave. The TDSW is resolved at the leading edge by a harmonic wavepacket moving with the linear group velocity. The non-classical TDSW exhibits features common to both dissipative and dispersive shock waves.

## 1. INTRODUCTION

Dispersive hydrodynamics encompass hyperbolic systems of equations regularized by dispersion rather than dissipation, modeling many physical media [14]. One of the most prominent features of these systems is a dispersive shock wave (DSW), in which gradient catastrophe at the purely hyperbolic level is resolved into an expanding, oscillatory wavetrain due to dispersive regularization. The standard or classical DSW can be modeled by the Korteweg-de Vries (KdV) equation

$$(1) \quad u_t + uu_x + \sigma u_{xxx} = 0,$$

where  $\sigma = \pm 1$ . A KdV DSW can be described by a slowly modulated, periodic traveling wave solution of (1) via Whitham theory [31], exhibiting two distinguished edges corresponding to a vanishing amplitude harmonic wavepacket and a vanishing wavenumber solitary wave (see schematic DSWs in Fig. 1). The canonical problem of interest is the Gurevich-Pitaevskii (GP) problem, whereby the long time dynamics for (1) with step initial data are considered [17]. The trailing ( $s_-$ ) and leading ( $s_+$ ) edge DSW velocities from the GP problem are distinct ( $s_- < s_+$ ) and differ from the single, classical shock velocity derived from the Rankine-Hugoniot jump conditions for the dispersionless Hopf equation

$$(2) \quad u_t + uu_x = 0.$$

Due to its dynamically expanding, distinct edge behavior, a DSW exhibits an orientation  $d$  and polarity  $p$ , identifying the location and polarity of the solitary wave edge. The DSW has  $d = +1$  ( $d = -1$ ) if the solitary wave edge is rightmost (leftmost) and  $p = +1$  ( $p = -1$ ) if the solitary wave edge is a wave of elevation (depression) with respect to its adjacent, slowly varying background (cf. Fig. 1). The linear dispersion

---

*E-mail address:* patrick.sprenger@colorado.edu, hoefer@colorado.edu.

*Date:* October 27, 2016.

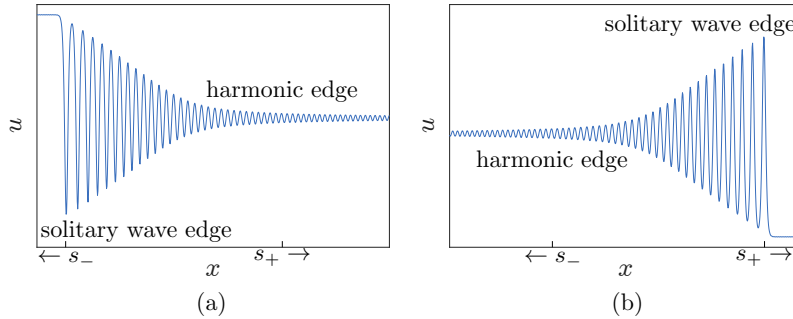


FIGURE 1. Expanding KdV-like DSWs ( $s_- < s_+$ ) for (a)  $\sigma = -1$  and (b)  $\sigma = +1$ , exhibiting dispersion curvature dependent orientation and polarity.

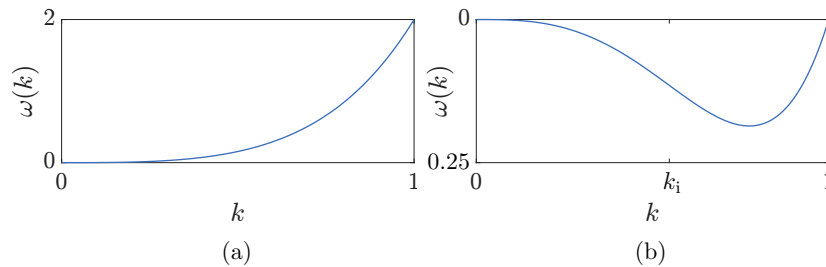


FIGURE 2. Dispersion relation (4) for the Kawahara equation (3) for  $\bar{u} = 0$ , (a)  $\sigma = -1$  and (b)  $\sigma = +1$ .

relation on a background  $\bar{u}$  for (1) is  $\omega(k, \bar{u}) = k\bar{u} - \sigma k^3$ . As shown in Fig. 1, the KdV DSW for eq. (1) has  $d = p = -\text{sgn } \omega_{kk} = \text{sgn } \sigma$ . We see that two fundamental KdV DSW properties, its orientation and polarity, are uniquely determined by the dispersion curvature, also referred to as the sign of dispersion. We refer to DSWs that resemble those in Fig. 1 as KdV-like or classical DSWs.

In this manuscript, we study DSWs in the presence of higher order dispersive effects via the fifth order KdV or Kawahara equation [22]

$$(3) \quad u_t + uu_x + \sigma u_{xxx} + u_{xxxxx} = 0,$$

where  $\sigma = \pm 1$ . The dispersion relation on background  $\bar{u}$

$$(4) \quad \omega(k, \bar{u}) = k\bar{u} - \sigma k^3 + k^5$$

is convex when  $\sigma = -1$  as depicted in Fig. 2(a).

Purely positive dispersion curvature suggests that Kawahara DSWs occurring in eq. (3) with  $\sigma = -1$  will be KdV-like and qualitatively similar to those in Fig. 1(a), which we indeed find to be the case (see Section 4.4). However, when  $\sigma = +1$ , the curvature of (4)

$$(5) \quad \omega_{kk} = -6k + 20k^3$$

changes sign at the inflection point  $k_i = \sqrt{3/10}$  as depicted in Fig. 2(b). Because DSWs are composed of modulated nonlinear waves with a range of wavenumbers from zero at the solitary wave edge to a characteristic, nonzero value at the harmonic edge [14], we expect fundamental differences in the DSW structure for eq. (3) when  $\sigma = +1$ . For example, the ‘‘classical’’ KdV DSWs described in the last paragraph feature very different structure (orientation, polarity) depending on the dispersion curvature. In this work, we aim to resolve the ways in which a single equation exhibiting both signs of dispersion curvature rectifies these differences.

Note that there is another source of non-convexity in dispersive hydrodynamic systems: a non-convex, hyperbolic flux. Such a flux is known to give rise to undercompressive shock waves and shock-rarefactions in hyperbolic systems theory and their analogues in dispersive hydrodynamics [13]. In contrast, the problem of non-convex dispersion has no hyperbolic correlate.

In the remainder of this introductory section, we review some relevant work on DSWs and solitary waves, then provide an overview of this work.

**1.1. Related work: dispersive shock waves.** Most DSW studies to date have focused upon dispersive hydrodynamic systems that exhibit either a purely convex or concave linear dispersion relation [14], with some recent exceptions [2, 6–9, 11, 15, 26]. The monograph [2] and paper [11] present numerical simulation results for the Kawahara equation (3) for both short-time [11] and long-time [2] dynamics. These simulation results resemble the types of shock waves we characterize in long-time in this work.

In [25], a scalar dispersive hydrodynamic model is shown to exhibit KdV-like DSWs until a critical jump height is reached corresponding to zero curvature at the harmonic wave edge. Further increase of the jump height results in the internal, self-interaction of the DSW or, as it was termed, DSW implosion. Zero curvature results in a local extremum of the group velocity that causes the harmonic edge waves within the DSW to interact with interior DSW waves of smaller wavenumber.

Qualitatively different dispersive hydrodynamics near zero dispersion were observed in Nonlinear Schrödinger (NLS) type models of intense light propagation through fibers [6–9, 26] and nematic liquid crystals [15]. In both cases, numerical simulations reveal that an essentially linear wavetrain’s phase speed is in resonance with the DSW’s solitary wave edge phase speed, leading to radiation. As the strength of higher order dispersion is increased, the DSW structure changes. Empirical observations suggest that in long time, the solitary wave edge exhibits a constant speed moving with the *classical* shock speed from the Rankine-Hugoniot conditions. This behavior is in stark contrast with KdV-like DSWs, whose speeds are determined through Whitham averaging [14].

**1.2. Related work: solitary waves.** Because DSWs can be considered spatially extended generalizations of solitary waves, it is helpful to briefly review the properties of solitary wave solutions of eq. (3), first computed by Kawahara [22]. Distinct structures emerge depending on the choice of the parameter  $\sigma$ . For  $\sigma = -1$ , the solitary waves are monotonically decaying from the peak. For  $\sigma = +1$ , there are non-monotonically decaying, depression solitary waves for velocities less than  $-\frac{1}{4}$  that are stable [5]. These oscillatory solitary waves bifurcate from the linear dispersion curve (4) when the phase and group velocities coincide [16]. The equality of phase and group velocities occurs only for non-convex dispersion  $\omega$ . For  $\sigma = +1$  and positive velocities, elevation solitary waves exist but are unstable due to a linear resonance [3, 29]. It is the Kawahara equation’s non-convex dispersion that leads to solitary waves embedded in the linear spectrum [30]. As we will demonstrate, non-convex dispersion yields similarly impactful effects on DSW dynamics.

**1.3. Overview of this work.** In Section 2, we derive the Kawahara equation (3) from a general dispersive Eulerian system via multiple-scales perturbation theory as a universal approximate model for weakly nonlinear dispersive waves when the coefficient of third order dispersion is small. The requisite conditions for higher order dispersive effects to be important are identified and the single free parameter  $\sigma$  in eq. (3) is related to the dispersive parameters of the original Eulerian system. We then consider water waves and nonlinear fiber optics as example dispersive hydrodynamic systems where this multiple scale method can be applied.

Section 3 reviews the numerical and asymptotic computation of Kawahara solitary wave solutions and their corresponding amplitude-speed relations for eq. (3). These solutions are then utilized to help describe the DSWs studied in Section 4.

In Section 4.1, we show that non-convex dispersion ( $\sigma = +1$ ) and sufficiently large jumps lead to a new coherent structure, a *traveling* DSW (TDSW). The TDSW is characterized by a non-monotonic, depression solitary wave trailing edge. Rather than complete a full oscillation, the solitary wave is partial and connects to a periodic nonlinear wavetrain. This portion of the TDSW is found to rapidly approach a *genuine traveling wave solution* of the Kawahara equation (3), connecting a constant to a periodic orbit. Approximate and numerical periodic solutions are obtained that yield the TDSW trailing edge speed as a function of jump height. The speed is found to be a generalization of the Rankine-Hugoniot jump condition of classical shock theory. The TDSW leading edge is found to move with the linear group velocity.

Small jumps for non-convex dispersion, examined in Section 4.2, involve long waves and weak fifth order dispersive effects. The resulting DSWs are perturbations of KdV-like DSWs with a leading edge elevation solitary wave that is in resonance with short, forward-propagating linear waves. These are referred to as *radiating* dispersive shock waves (RDSWs). RDSW properties are determined DSW fitting theory.

Moderate jumps for non-convex dispersion are examined in Section 4.3 where more complex dynamics are observed. This is the regime that straddles the linear dispersion inflection point  $k_i$ , corresponding to unsteady, crossover behavior where we observe strong forward and backward propagation of waves. We equate this regime with wave speeds in the solitary wave “band gap” where Kawahara solitary waves do not exist but nonlinear periodic traveling waves do.

Convex dispersion ( $\sigma = -1$ ) is considered in Section 4.4 where we observe a classical KdV-like DSW. We apply DSW fitting theory in order to determine the amplitude and speed of the trailing solitary wave and the wavenumber at the leading edge as a function of the initial jump height.

Finally, we conclude the manuscript in Section 5 with some discussion and broader perspectives on our findings.

## 2. UNIVERSALITY OF THE KAWAHARA EQUATION

We consider a general dispersive Eulerian system of equations given in non-dimensional form by

$$(6) \quad \rho_t + (\rho u)_x = D_1[\rho, u]_x,$$

$$(7) \quad (\rho u)_t + (\rho u^2 + P(\rho))_x = D_2[\rho, u]_x,$$

where  $\rho = \rho(x, t)$  corresponds to the fluid density,  $u = u(x, t)$  the fluid velocity, and the pressure law is given by  $P(\rho)$ . We assume strict hyperbolicity  $P'(\rho) > 0$  and genuine nonlinearity  $[\rho^2 P'(\rho)]' > 0$  of the dispersionless system ((6), (7) with  $D_{1,2} = 0$ ) so that weakly nonlinear dynamics exhibit quadratic, convex flux [13]. The differential operators  $D_1, D_2$  acting on  $\rho, u$  in (6) and (7) are assumed to be of the second order or higher, yielding a real valued dispersion relation. The dispersion is calculated by assuming a small amplitude linear wave oscillating about the background state  $(\rho_0, u_0)$ :  $\rho = \rho_0 + Ae^{i\theta}$ ,  $u = u_0 + Be^{i\theta}$  where  $\theta = kx - \omega t$  and  $|A|, |B| \ll 1$  are of the same order. Substitution of this ansatz into (6) and (7) yields a homogeneous system of linear equations for  $A$  and  $B$  that are only solvable for two distinct frequency branches  $\omega_{\pm}(k)$ , the dispersion relation. The dispersion relation exhibits the long wave ( $0 < k \ll 1$ ) behavior

$$(8) \quad \omega_{\pm}(k) = u_0 k \pm \left( c_0 k + \mu k^3 + \gamma k^5 + o(k^5) \right),$$

where  $c_0 = \sqrt{P'(\rho_0)}$  is the long wave speed of sound and  $\mu, \gamma$  are the third and fifth order dispersion coefficients, respectively. In general, these coefficients will depend on  $\rho_0, u_0$  and possibly other parameters. We are interested in the asymptotic balance of third and fifth order dispersion, which can result when the coefficient of third order dispersion  $\mu$  is sufficiently small. Since  $k$  is inversely proportional to the characteristic length scale  $L$ , called the *coherence length* [14], then fifth order dispersion is important when  $\mu \sim 1/L^2$ . The presence of both third and fifth order dispersion with comparable magnitudes can result in a change in the dispersion sign.

We now seek approximate uni-directional solutions to the system (6) and (7) via multiple-scales in the form

$$\begin{aligned} \tau &= \epsilon^{5/4} t, \quad \eta = \epsilon^{1/4} (x - (u_0 + c_0)t), \\ \rho &= \rho_0 + \epsilon \rho_1(\eta, \tau) + \epsilon^{3/2} \rho_2(\eta, \tau) + \epsilon^2 \rho_3(\eta, \tau) + o(\epsilon^2), \\ u &= u_0 + \epsilon u_1(\eta, \tau) + \epsilon^{3/2} u_2(\eta, \tau) + \epsilon^2 u_3(\eta, \tau) + o(\epsilon^2). \end{aligned}$$

Note the non-integer powers of  $\epsilon$ , chosen so that quadratic nonlinearity will balance the third and fifth order dispersion terms. In other words, we assume the maximal balance scaling

$$(9) \quad \mu = \epsilon^{1/2} \tilde{\mu}, \quad \tilde{\mu} = \mathcal{O}(1).$$

We also assume the boundary conditions

$$(10) \quad \rho(x, t) \rightarrow \rho_0, \quad u(x, t) \rightarrow u_0, \quad x \rightarrow \infty.$$

Substituting this expansion into (6), (7) and using (10), and applying a standard multiple scales approach as in [31] we have  $\rho_1 = \frac{\rho_0}{c_0} u_1$ , where  $u_1$  satisfies the Kawahara equation

$$(11) \quad u_{1,\tau} + \alpha u_1 u_{1,\eta} - \tilde{\mu} u_{1,\eta\eta\eta} + \gamma u_{1,\eta\eta\eta\eta} = 0.$$

Equation (11) can be put in the normalized form (3) by use of the scaled variables

$$(12) \quad x' = \left| \frac{\tilde{\mu}}{\gamma} \right|^{1/2} \eta, \quad t' = \gamma \left| \frac{\tilde{\mu}}{\gamma} \right|^{5/2} \tau, \quad u' = \frac{\alpha\gamma}{\tilde{\mu}^2} u,$$

and then dropping primes. The key parameter in the Kawahara equation (3) that encapsulates the competition between third and fifth order dispersion is

$$(13) \quad \sigma = -\text{sgn}(\tilde{\mu}\gamma).$$

We now apply these results to specific model equations from water waves and fiber optics.

**2.1. Water waves.** In order to accurately capture the competing effects of third and fifth order dispersion in water waves, we use the recently derived extended Green-Naghdi or Serre equations [28] with surface tension effects incorporated as in the generalized Serre (gSerre) equations [10], yielding the extended, generalized Serre or egSerre equations. The corresponding dispersive operators and general pressure law in (6) and (7) for egSerre are

$$(14) \quad \begin{aligned} D_1(\rho, u) &= 0, \\ D_2(\rho, u) &= \frac{\rho^3}{3} (u_{xt} + uu_{xx} - u_x^2) - B \left[ \frac{1}{2} \rho_x^2 - \rho \rho_{xx} \right] + \left[ \frac{\rho^5}{45} (u_{xxt} + uu_{xxx} - 5u_x u_{xx}) \right]_x - 3\rho^5 u_{xx}^2, \\ P(\rho) &= \frac{\rho^2}{2}, \end{aligned}$$

where the dependent variables  $\rho(x, t)$  and  $u(x, t)$  are the nondimensional water surface height and vertically averaged horizontal velocity component, respectively. The bond number,  $B$ , is a dimensionless parameter that quantifies the strength of surface tension relative to gravity. The dispersion relation for eqs. (6), (7) with (14) on the background  $\rho_0 = 1$  and  $u_0 = 0$  has the long wave expansion

$$(15) \quad \omega(k) = k + \frac{1}{6}(3B - 1)k^3 + \frac{1}{360}(19 - 30B - 45B^2)k^5 + o(k^5),$$

which agrees with the long wave expansion of the full water wave dispersion relation [21]

$$(16) \quad \omega = [(1 + Bk^2)k \tanh(k)]^{1/2}.$$

The coefficients for the Kawahara equation (11) are then

$$\mu = \frac{1}{6}(1 - 3B), \quad \gamma = \frac{1}{360}(19 - 30B - 45B^2), \quad \alpha = \frac{3}{2}.$$

As noted in our derivation, the Kawahara equation is valid when  $\mu$  is small, therefore we are considering  $B$  close to  $1/3$ . Note that we have also assumed that  $\gamma = \mathcal{O}(1)$ . Since  $\gamma$  is zero when  $B = (2\sqrt{30} - 5)/15 \approx 0.40$ , we require  $B < 0.4$  for the asymptotic validity of the scaled Kawahara equation (3) with parameter

$$(17) \quad \sigma = -\text{sgn}(\mu\gamma) = \text{sgn}(1 - 3B).$$

When  $B < 1/3$ , gravity effects dominate surface tension effects and we have  $\sigma = +1$ . Neglecting the fifth order term, the KdV equation (1) therefore exhibits negative dispersion with positive polarity and orientation DSWs as in Fig. 1(b).

If we had neglected the higher order terms from the egSerre equations and just used the gSerre equations, the dispersion would not agree with the long wave expansion for the full water waves dispersion relation (16) to fifth order. As such, it is necessary for one to include *both* the effects that result in small third order dispersion as well as higher order terms to maintain the required asymptotic balance. This suggests that one should consider with some caution the applicability of the gSerre model to physical water wave problems when  $B$  is near  $\frac{1}{3}$ .

In [19], the authors derived the Kawahara equation directly from the Euler equations as a model for shallow water waves for Bond number near  $\frac{1}{3}$ . We have now demonstrated an alternative derivation based on the egSerre equations via their interpretation as dispersive Eulerian hydrodynamic equations.

**2.2. Nonlinear fiber optics.** The effect of higher order dispersive terms in the Nonlinear Schrödinger equation and associated experiments were studied in the series of papers [6–9, 26] within the context of light propagation in optical fibers. See also [2] for applications in continuum mechanics. The equation of interest is a higher order NLS equation

$$(18) \quad i\psi_t + \frac{1}{2}\psi_{xx} + i\frac{\beta_3}{6}\psi_{xxx} - |\psi|^2\psi = 0,$$

where  $\psi$  is the complex envelope of a weakly nonlinear carrier wave and  $\beta_3$  is a parameter modeling higher order dispersive effects in the fiber. The variables  $x, t$  are used here to maintain consistency with (6) and (7) but physically correspond to nondimensionalized time and negative distance along the fiber, respectively. The Madelung transformation  $\psi = \sqrt{\rho}e^{i\phi}$ ,  $u = \phi_x$  can be utilized to write eq. (18) as a generalized dispersive Eulerian system

$$\begin{aligned} \rho_t + \left( \rho u - \frac{1}{2}\beta_3\rho u^2 \right)_x &= D_1[\rho, u]_x, \\ (\rho u)_t + \left( \rho u^2 - \frac{1}{2}\beta_3\rho u^3 + \frac{1}{2}\rho^2 \right)_x &= D_2[\rho, u]_x, \end{aligned}$$

where

$$\begin{aligned} D_1[\rho, u] &= \beta_3 \left( \frac{1}{6}\rho_{xx} - \frac{1}{8}\frac{\rho_x^2}{\rho} \right), \\ D_2[\rho, u] &= \frac{1}{4}\rho (\log(\rho))_{xx} + \frac{\beta_3}{12} \left( \frac{9\rho_x^2 u}{2\rho} - 5\rho_{xx}u - \rho_x u_x - 2\rho u_{xx} \right). \end{aligned}$$

Utilizing the same method as our general derivation of the Kawahara equation for dispersive Eulerian equations, we obtain eq. (11) with coefficients

$$\begin{aligned} \alpha &= \frac{3 - \beta_3 (6u_0 - 3u_0^2\beta_3 + \sqrt{\rho_0 - \rho_0 u_0 \beta_3})}{2(1 - u_0\beta_3)}, \\ \mu &= \frac{(7u_0\beta_3 - 3)\sqrt{\rho_0 - \rho_0 u_0 \beta_3}}{24\rho_0}, \\ \gamma &= \frac{\sqrt{\rho_0 - \rho_0 u_0 \beta_3} (-9 + 51u_0\beta_3 + 16\rho_0\beta_3^2 - 91u_0^2\beta_3^2 + 49u_0^3\beta_3^3)}{1152\rho_0^2(u_0\beta_3 - 1)}. \end{aligned}$$

Interestingly, a nonzero background velocity  $u_0$  is required in order to achieve a balance between third and fifth order dispersion. We note that the numerical simulations in [6] consider the cases  $\rho_0 = 0.5$ ,  $u_0 \in (-0.586, -0.543)$ , and  $\beta_3 \in (-0.35, -1)$ , corresponding to  $\sigma = -\text{sgn}\mu\gamma = +1$ , the non-convex dispersion case.

**2.3. Other systems.** The Kawahara equation (3) was derived in the case of intense light propagation through nematic liquid crystals [15]. The governing equation is a non-local NLS-type equation. The authors numerically observed the generation of the crossover regime (see Section 4.3) and related its qualitative features to those of the full model equations, where a more detailed numerical and asymptotic analysis were carried out.

We also note that, with the development of spin-orbit coupled Bose-Einstein condensates (BECs) [23, 24], it is possible to “engineer” the dispersion experienced by the wave functions of two nonlinearly coupled spin states. In a cigar shaped trap where the BEC is approximately one-dimensional, the mean-field dynamics may be modeled by two coupled NLS equations (see, e.g., [1] and references therein), which exhibit non-convex dispersion.

Another novel application of the Kawahara equation is in the description of shallow water waves under ice cover when the Young modulus of ice is sufficiently large [20, 27].

### 3. SOLITARY WAVE SOLUTIONS

The structure of solitary wave solutions to the Kawahara equation (3) are well known [3, 16, 22]. In what follows, we outline relevant properties of these solutions. When  $\sigma = +1$ , solitary waves are unstable when embedded in the continuous spectrum, i.e., when they exhibit a linear resonance for velocities  $c > 0$  [30].

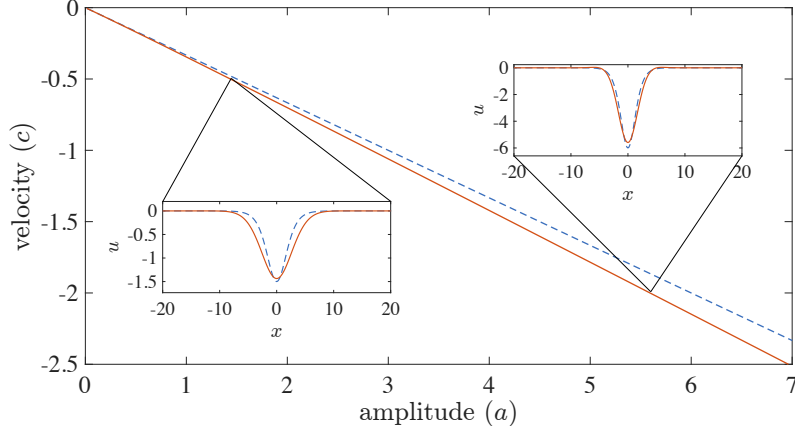


FIGURE 3. Solitary wave profiles and speed-amplitude relation for the Kawahara equation with  $\sigma = -1$  (solid) and KdV equation (dashed).

However, there are stable, non-monotonic solitary waves outside the continuous spectrum when  $c < -\frac{1}{4}$  [5]. Our investigation of solitary wave solutions focuses upon their numerical and asymptotic calculation. A key quantity of interest is the amplitude-speed relation for these solitary waves, which will prove useful in the study of DSWs.

We seek solutions of eq. (3) in the form  $u(x, t) = f(\xi; c)$ ,  $\xi = x - ct$ . Upon integrating once, we obtain

$$(19) \quad -cf + \frac{1}{2}f^2 + \sigma f'' + f^{(4)} = 0,$$

where decay of  $f(\xi; c)$  and its first four derivatives eliminates the integration constant. The nonlinear equation (19) is solved via the Newton Conjugate Gradient method [32] or with Matlab's boundary value solver `bvp5c` for the solitary wave profile  $f$  corresponding to the speed  $c$ . For comparative purposes, we recall the well-known soliton solution of the KdV equation (1)

$$(20) \quad f(\xi; c) = a\sigma \operatorname{sech}^2\left(\sqrt{\frac{|a|}{12}}\xi\right), \quad c(a) = \frac{a\sigma}{3}.$$

The monotonic Kawahara solitary waves are well-approximated by the KdV solution (20) in the small amplitude regime [3]. Here, monotonic refers to the decay profile on either side of the solitary wave peak—a convention presented in [22]. Higher order dispersion acts as a small perturbation to the KdV solitary wave. This effect can be understood by integrating (19) again to obtain

$$(21) \quad -\frac{c}{2}f^2 + \frac{1}{6}f^3 + \frac{\sigma}{2}(f')^2 + f'f''' - \frac{1}{2}(f'')^2 = 0.$$

Evaluating at the solitary wave extremum  $\xi = 0$  yields the correction to the KdV speed-amplitude relation (20)

$$(22) \quad c(a) = \frac{a\sigma}{3} - \left(\frac{f''(0; c)}{a}\right)^2 = \frac{a\sigma}{3} - \frac{a^2}{36} + \mathcal{O}(a^3),$$

The approximate expression is obtained by inserting the KdV soliton solution (20). The speed correction in (22) is strictly negative, independent of  $\sigma$ .

The Kawahara solitary wave amplitude-speed relation and sample solitary waves for the case of convex dispersion  $\sigma = -1$  are shown in Fig. 3.

In the regime of non-convex dispersion,  $\sigma = +1$ , there are two distinct branches of solitary wave solutions depicted in Fig. 4. The case  $c > 0$  corresponds to KdV-like elevation waves. We note that the Kawahara speed-amplitude relation for  $\sigma = +1$  more rapidly departs from the KdV relation in Fig. 4 than in Fig. 3 for  $\sigma = -1$ . These solutions are embedded in the continuous wave spectrum, consisting of all possible linear phase speeds  $\omega/k = -k^2 + k^4 > -\frac{1}{4}$  and depicted on the vertical axis in Fig. 4. It was observed in [3] that a resonance between the solitary wave and small amplitude waves with the same phase speed occurs. This

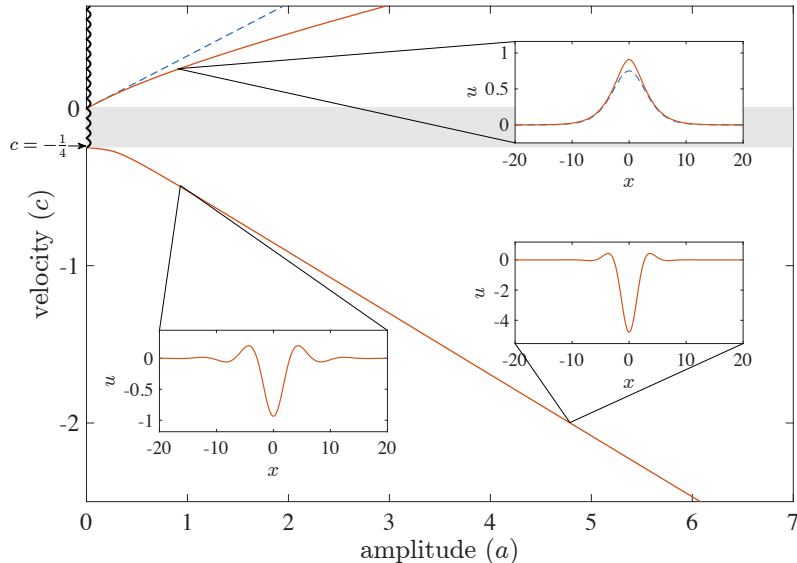


FIGURE 4. Solitary wave profiles and speed-amplitude relation for the Kawahara equation with  $\sigma = +1$  (solid) and KdV equation (dashed). The linear wave spectrum is denoted on the vertical axis by the thick black curve. The “band gap” where no solitary waves exist is the shaded region.

radiation decreases the amplitude of the solitary wave core as the solution propagates. This is indicative of a general property of embedded solitary waves [30].

When  $c < -\frac{1}{4}$ , the solitary waves are depression waves with non-monotonic profiles. In [5], it was shown that this solution branch is stable. The linearization of the solitary wave equation (19) about zero results in a linear, constant coefficient differential equation with characteristic roots

$$r_{\pm}^2 = \frac{-1 \pm \sqrt{1 + 4c}}{2},$$

that are complex with nonzero real part for  $c < -\frac{1}{4}$  and purely imaginary for  $-\frac{1}{4} < c < 0$ . Consequently, solitary waves with negative velocity can only exist for  $c < -\frac{1}{4}$ . A more detailed, asymptotic analysis of weakly nonlinear, modulated waves for  $0 < -\frac{1}{4} - c \ll 1$  demonstrates a bifurcation of oscillatory, envelope solitary waves, hence the non-monotonic profiles in Fig. 4 for  $c < -\frac{1}{4}$  [5, 16]. Our numerical computations yield only nonlinear periodic traveling waves for velocities  $-\frac{1}{4} < c < 0$  so we call this region the *solitary wave band gap*.

#### 4. DISPERSIVE SHOCK WAVES

In this section, we study DSWs in the Kawahara equation (3), fundamental coherent structures in dispersive hydrodynamics. Generically, DSWs arise in the long time evolution of initial data that leads to gradient catastrophe or wavebreaking in the dispersionless limit. The canonical GP problem of dispersive hydrodynamics is to consider the evolution of step initial data

$$(23) \quad u(x, 0) = \begin{cases} 0, & x < 0, \\ -\Delta, & x \geq 0 \end{cases}, \quad \Delta \in \mathbb{R}.$$

More general, two-parameter initial conditions can be obtained by utilizing the Galilean invariance of the Kawahara equation. First, we recall the behavior of solutions to the dispersionless Hopf equation (2) with initial data (23). When  $\Delta < 0$ , a rarefaction weak solution exists and approximates the dispersive hydrodynamics of eq. (3) subject to small dispersive corrections. However, when  $\Delta > 0$ , the Hopf equation (2) admits a weak discontinuous shock wave solution with shock speed

$$(24) \quad s = -\frac{1}{2}\Delta$$

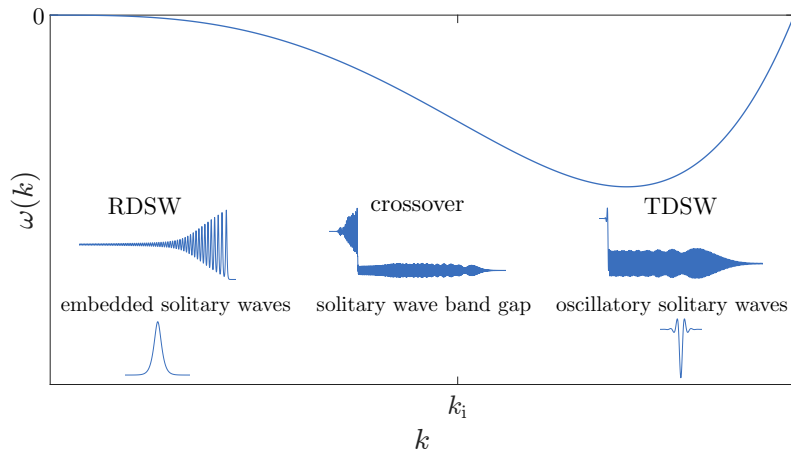


FIGURE 5. Non-convex Kawahara dispersion relation for  $\sigma = +1$  along with example numerical simulations for step initial data. The RDSW, crossover regime, and TDSW can be identified with properties of the dispersion curvature and the existence of solitary wave structures.

deduced from the Rankine-Hugoniot (RH) jump conditions. The additional dispersive terms in the Kawahara equation act as a singular perturbation and a different approach must be explored.

In what follows, we use careful numerical computations of the GP problem for the Kawahara equation (3) with initial data (23) as one of our analysis tools. Motivated by the results of these simulations, we also implement traveling wave computations and asymptotic analyses that favorably compare with the numerical results.

We utilize an integrating factor pseudospectral discretization in space with 4th order Runge-Kutta (RK4) temporal evolution. The method is a generalization of the method applied to the modified KdV equation in [13] where  $u_x$  is assumed to be localized within the truncated spatial domain so that a Fourier series expansion is possible. We temporally evolve  $u_x$  using RK4 and the nonlinear term is computed using a pseudospectral approach. The numerical simulations were performed on a spatial domain of length  $L = 10^5$  and the location of the initial, tanh smoothed discontinuity appropriately chosen to minimize wave-boundary interactions. It is the fast propagation of small amplitude dispersive waves due to fifth order dispersion that necessitate such a large domain. Various aspects of the approximate solutions were tested in order to ensure robustness of the numerical method as well as accuracy of the solution. In particular, all solutions reported exhibit boundary deviations less than  $10^{-3}$ . The Fourier coefficients of  $u_x$  all decay to  $10^{-10}$  or less in normalized amplitude and the mass satisfies the conservation property

$$\int_0^L u(x, t) dx - \int_0^L u(x, 0) dx = -\frac{t\Delta^2}{2},$$

maintained below a relative error of  $10^{-3}$ , which was only approached for long times  $t = O(100)$  as a result of the small amplitude oscillations at the boundaries. Typical simulations presented in this section maintained a relative error on the order of  $10^{-4}$ .

We begin our investigation of Kawahara DSWs with the non-convex dispersion case  $\sigma = +1$ . The dynamics can be grouped into three qualitatively distinct regimes, loosely characterized by the dispersion relation and soliton solutions. These regimes are identified in Fig. 5 along with representative numerical solutions. Small to large jump heights generate predominantly small to large wavenumbers, respectively. The regime of negative dispersion curvature can be associated with elevation solitary waves embedded in the linear spectrum, hence naturally appear as a constituent part of radiating DSWs. Oscillatory, depression solitary waves result from non-convex dispersion and are associated with traveling DSWs. The crossover regime straddles the dispersion inflection point and the solitary wave band gap.

We now undertake a more thorough analysis of the large amplitude regime and the generation of non-classical traveling DSWs.

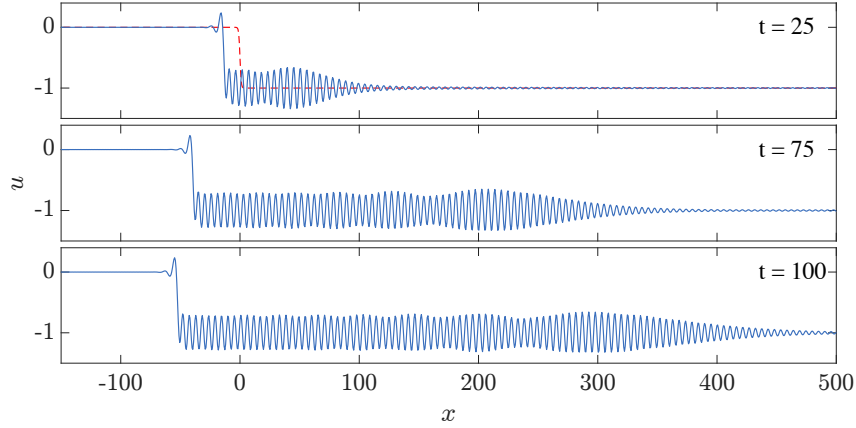


FIGURE 6. Kawahara traveling DSW resulting from the initial step  $\Delta = 1$  for the non-convex case  $\sigma = +1$ . Initial data is shown in the top figure with the dashed curve.

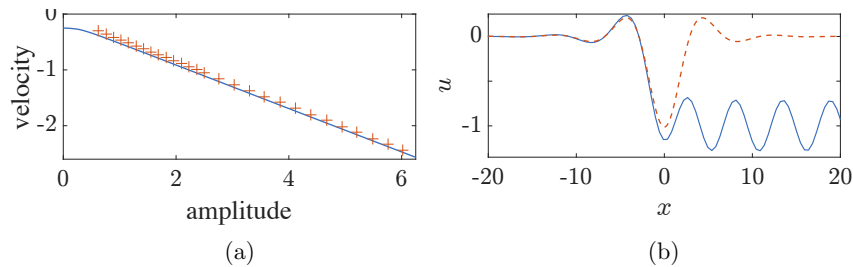


FIGURE 7. Trailing edge comparison with Kawahara ( $\sigma = +1$ ) solitary waves. a) Computed TDSW (pluses) and solitary wave (solid) amplitude-speed relations. b) Overlay of solitary wave on TDSW leading edge with  $\Delta = 1$ .

**4.1. Non-convex dispersion with large jumps: TDSWs.** We now assume that  $\Delta$  is sufficiently large in order to give rise to a non-classical traveling DSW. The crossover to this large jump regime will be made more precise in Section 4.3. Figure 6 is a simulation with initial jump  $\Delta = 1$ . We observe a sharp, non-monotonic transition from a constant to a nearly periodic wavetrain. The wavetrain exhibits some envelope modulations that eventually terminate at the leading edge with small amplitude oscillations. This coherent wavetrain is the TDSW. We begin our analysis by verifying two DSW-like properties of the dynamics: 1) a near solitary wave trailing edge, 2) a harmonic wave leading edge.

First, we plot the amplitude-speed relations for both the trailing edge of TDSWs with varying  $\Delta$ , extracted from numerical simulations, and Kawahara solitary waves in Fig. 7(a), exhibiting excellent agreement. Furthermore, in Fig. 7(b), we overlay a Kawahara depression solitary wave with the same speed as the TDSW trailing edge. A portion of the solitary wave correctly captures the non-monotonic structure of the rapid transition. Therefore, we can identify TDSWs with the non-monotonic solitary wave branch of solutions (cf. Fig. 4).

Next, we numerically extract the wavenumber  $\bar{k}$  of the TDSW wavetrain just to the right of the solitary wave trailing edge for varying  $\Delta$  by averaging the wavenumber of 10 oscillations immediately to the right of the partial solitary wave after the TDSW is developed. The leading edge velocity is also numerically extracted and compared with the Kawahara group velocity evaluated at  $\bar{k}$  in Fig. 8. We observe excellent agreement. Based on these two numerical observations, we see that the TDSW exhibits solitary and harmonic wave edges, typical of classical DSWs [14]. But that is where the analogy ends. As we will now show, the TDSW exhibits unique, non-classical features.

**4.1.1. TDSW trailing edge traveling wave.** Further scrutiny of the trailing edge shows what appears to be the development of a nonlinear, periodic wavetrain co-moving with the partial solitary wave. The approximately

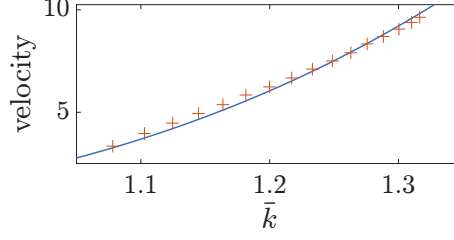


FIGURE 8. Comparison of TDSW harmonic leading edge speed extracted from numerical simulations with the linear group velocity. Leading edge velocities (shifted by the background  $-\Delta$ ) versus the wavenumber  $\bar{k}$  near the trailing edge extracted from numerical simulations (pluses). The linear group velocity  $\omega_k(\bar{k}, -\Delta) + \Delta$  is also depicted (solid).

periodic wavetrain oscillates about the mean value  $-\Delta$ . This suggests seeking a one-parameter family of Kawahara traveling waves  $u(x, t) = f(\xi)$ ,  $\xi = x - ct$  subject to the boundary conditions (BCs)

$$(25) \quad \text{equilibrium BCs: } \begin{cases} \lim_{\xi \rightarrow -\infty} f(\xi) = f'(\xi) = f''(\xi) = f'''(\xi) = f''''(\xi) = 0, \end{cases}$$

$$(26) \quad \text{periodic orbit BC: } \begin{cases} \lim_{\xi \rightarrow \infty} f(\xi) = F(\xi), & F(\xi + P) = F(\xi), & \xi \in \mathbb{R}, \\ \frac{1}{P} \int_0^P F(\xi) d\xi = -\Delta, \end{cases}$$

where  $P$  is the wavetrain's period. Inserting the traveling wave ansatz into the Kawahara equation (3), we can integrate once and apply the boundary conditions at  $\xi \rightarrow -\infty$  to obtain the same fourth order ODE (19) we obtained for solitary waves. The traveling wave has two free parameters  $c$  and  $P$  that should be uniquely determined by the jump  $\Delta$ . One relation is the mean requirement in (26). Another relation is obtained by integrating (19) again and applying the boundary conditions (25) to obtain the *zero energy integral* (21).

To determine the periodic orbit  $F(\xi)$ , we begin with an approximate, weakly nonlinear calculation. We consider a small amplitude  $0 < \bar{a} \ll 1$  expansion of  $F$  and  $c$  as in the classical Stokes expansion [31]

$$\begin{aligned} F(\xi) &= F_0(\theta) + \bar{a}F_1(\theta) + \bar{a}^2F_2(\theta) + \dots, & \theta &= \bar{k}\xi, \\ c &= c_0 + \bar{a}^2c_2 + \dots, \end{aligned}$$

where  $\bar{k} = 2\pi/P$  is the wavenumber of the periodic orbit. Inserting the expansion into (19) and carrying out a standard perturbation calculation, we find

$$(27) \quad F = F_0 + \bar{a} \cos \theta + \bar{a}^2 \left( 2c_2 - \frac{1}{2F_0} - \frac{1}{2 - 16\bar{k}^2 + 64\bar{k}^4} \cos(2k\xi) \right) + o(\bar{a}^2)$$

$$(28) \quad c = \frac{F_0}{2} + \bar{a}^2c_2 + o(\bar{a}^2)$$

$$(29) \quad \bar{k}^2 = \frac{1 + \sqrt{1 - 2F_0}}{2}$$

where

$$(30) \quad c_2 = \frac{3F_0 - 16\bar{k}^2 + 64\bar{k}^2}{4F_0^2 - 64\bar{k}^2 + 128\bar{k}^4},$$

and  $F_0$  is a constant to be determined.

The mean requirement (26) applied to (27) yields

$$(31) \quad F_0 + \bar{a}^2 \left( 2c_2 - \frac{1}{2F_0} \right) = -\Delta.$$

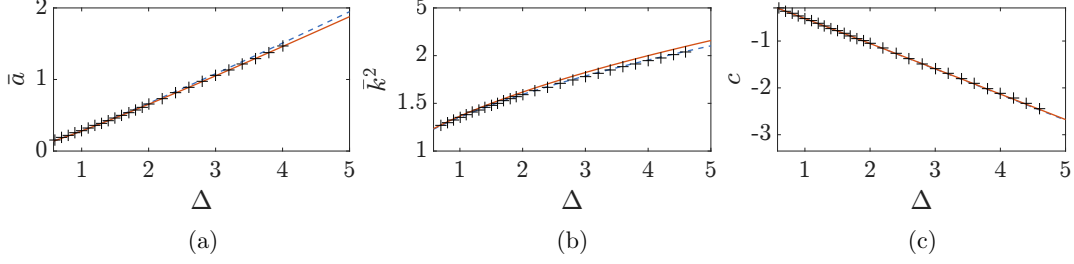


FIGURE 9. Comparisons of asymptotic predictions of nonlinear wavetrain features: (a) the amplitude of the nonlinear wavetrain, (b) the square of the wavenumber of the nonlinear wavetrain, and (c) the speed of the traveling wave. All figures compare values from computed traveling wave solutions (solid), asymptotic predictions (dashed), and data extracted from numerical simulations of the GP problem (pluses).

To account for the  $\mathcal{O}(\bar{a}^2)$  terms in the mean, the background  $F_0$  is expanded in the parameter  $\bar{a}$  in the form  $F_0 = F_{0,0} + \bar{a}^2 F_{0,2} + o(\bar{a}^2)$ . Substitution of the asymptotic expansion yields

$$(32) \quad F_0 = -\Delta - \frac{\bar{a}^2}{2} \left( \frac{29\Delta + 24\sqrt{2\Delta + 1} + 24}{\Delta^2 + 16\Delta + 8\sqrt{2\Delta + 1} + 8} + \frac{1}{\Delta} \right),$$

effectively canceling the  $\mathcal{O}(\bar{a}^2)$  mean terms in (27). The only remaining free parameter is the wave amplitude  $\bar{a}$ , which can be determined by inserting the expansion (27) into the zero energy estimate (21) and evaluating at the wave maximum  $\theta = 0$ , which yields

$$(33) \quad \bar{a} = \frac{\Delta^{3/2}}{\sqrt{3 + \frac{9\Delta}{2} + 3\sqrt{2\Delta + 1}}}.$$

Combining (32), (30), (29). and (28), we obtain an amplitude correction to the speed of the traveling wave

$$(34) \quad c = -\frac{\Delta}{2} + \frac{\bar{a}^2}{4\Delta},$$

and the square wavenumber of the wavetrain at leading order is given by

$$(35) \quad \bar{k}^2 = \frac{1 + \sqrt{1 + 2\Delta}}{2}.$$

We verify the accuracy of these approximate solutions by directly computing mean  $-\Delta$ , zero energy periodic orbits satisfying eqs. (19) and (21) using Matlab's boundary value solver `bvp5c`. Figure 9 shows the estimated and computed parameters  $c$ ,  $\bar{a}$ , and  $\bar{k}$  for mean  $-\Delta$  periodic solutions. Excellent agreement is obtained for all values of  $\Delta$  for which the traveling wave solutions were calculated.

What we have shown is that, if a Kawahara traveling wave satisfying the BCs (25) and (26) exists, its speed  $c$  is determined by the boundary conditions and, in particular, the jump height  $\Delta$ . The first term in the velocity expansion  $c_0 = -\Delta/2$  is the Rankine-Hugoniot jump condition (24) for classical shock waves. Therefore, we identify the traveling wave velocity  $c$  as a *generalized Rankine-Hugoniot condition* (gRH) given in (34).

We now directly compute traveling waves satisfying the BCs (25), (26) and the zero energy integral (21). Given a jump height  $\Delta$  and an associated zero energy far-field periodic solution  $F(\xi)$ , we compute solutions of the fourth order equation (19) with the four boundary conditions

$$(36) \quad f(0) = f'(0) = 0, \quad f(L) = F(0), \quad f''(L)^2 = -cf(L)^2 + \frac{1}{3}f(L)^3,$$

where  $L$  is sufficiently large so that the periodic orbit BC  $F(\xi)$  has been reached. The third condition in (36) evaluates the periodic orbit at a maximum. The fourth condition evaluates the zero energy integral (32) at a maximum. We use Matlab's collocation method `bvp5c` with an initial guess extracted from the numerical simulation depicted in Fig. 6 that is then used to perform continuation to other values of  $\Delta$ .

The computed traveling wave solution for  $\Delta = 1$  is superimposed on the TDSW determined by long-time integration of the GP problem, also for  $\Delta = 1$ , in Fig. 10(a). Sufficiently near the TDSW trailing edge, the

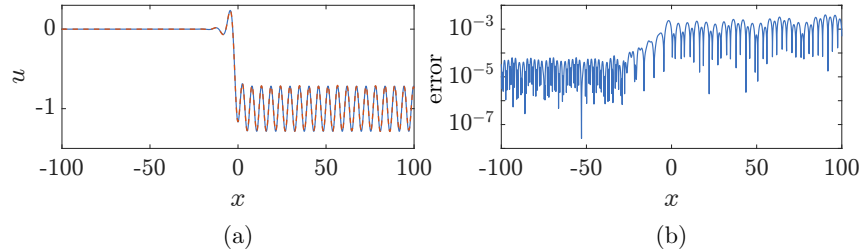


FIGURE 10. (a) Superimposed traveling wave solution to the dynamical system (19) with boundary conditions (36) (solid) on a TDSW computed from the GP problem with  $\Delta = 1$  (dashed) at  $t = 150$ . (b) Absolute error between the two solutions.

two solutions are indistinguishable. Figure 10(b) shows an absolute difference of at most  $10^{-3}$  between these two solutions. This demonstrates that the TDSW trailing edge rapidly approaches a traveling wave, hence the terminology *traveling* DSW.

We further examine properties of the TDSW by comparing the numerically extracted trailing edge velocity,  $s_-$ , of the TDSW and the speed of the computed traveling wave,  $c$ , in Fig. 9(a). We also compare the amplitude of the TDSW trailing edge wavetrain to the amplitude of the computed nonlinear wavetrain in the traveling wave  $\bar{a}$  in Fig. 9(b). Both properties agree over a wide range of  $\Delta$ .

Our traveling wave computations suggest that the solution is a heteroclinic connection between the equilibrium  $f = 0$  and the mean  $-\Delta$  periodic orbit  $f = F(\xi)$ . We are able to accurately compute such solutions for  $\Delta > \Delta_{cr} \approx 0.58$ , suggesting a threshold for their existence. Such a threshold is consistent with the speed requirement  $c < -\frac{1}{4}$  for non-monotonic Kawahara solitary waves (cf. Fig. 4), of which the TDSW trailing edge is approximately composed. We will examine the relationship between  $\Delta_{cr}$  and the crossover to the TDSW regime in Section 4.3.

**4.2. Non-convex dispersion with small jumps: RDSWs.** We now consider the non-convex case of eq. (3) ( $\sigma = +1$ ) in the small jump regime,  $0 < \Delta \ll 1$ . Introducing the scaling

$$(37) \quad u = \Delta U, \quad X = \Delta^{1/2}x, \quad T = \Delta^{3/2}t,$$

into eq. (3) results in a perturbed KdV equation

$$(38) \quad U_T + UU_X + U_{XXX} = -\Delta U_{XXXX}.$$

In the scaled variables (37), the initial conditions (23) become

$$(39) \quad U(X, 0) = \begin{cases} 0 & X < 0, \\ -1 & X > 0 \end{cases}.$$

Numerically, we evolve the scaled equation (38) subject to (39) but report the results for the unscaled field  $u(x, t)$  through (37). Numerical results are shown in Fig. 11. Sufficiently small jumps lead to KdV-like, classical DSWs as Fig. 11(a) with  $\Delta = 0.06$  attests. In this long-wave regime, the Kawahara linear dispersion relation (4) is essentially concave (cf. Fig. 2) so that the resulting DSWs exhibit positive polarity and orientation. The DSW leading edge is well approximated by an elevation Kawahara solitary wave as shown in Fig. 11(c). However, due to the embedding of the elevation solitary waves in the continuous spectrum, the solitary wave emits small amplitude radiation ahead of the shock, a phenomenon demonstrated in Fig. 11(b). This DSW resonant radiation has also been observed in NLS-type models [6, 15], so we introduce the nomenclature *radiating* DSW (RDSW) to describe this phenomenon.

For the analysis of RDSWs, one could consider Whitham theory [31] for the full Kawahara equation. We directly apply El's DSW fitting method [12] (see also [14]), which assumes the applicability of Whitham theory. Under appropriate conditions, the method yields the leading and trailing edge speeds as functions of the jump  $\Delta$ . Additional macroscopic DSW properties that can be obtained are the solitary wave edge amplitude and the harmonic wave edge characteristic wavenumber. The fitting method can be carried out with knowledge of only the linear dispersion relation and the solitary wave amplitude-speed relation, both of which we know exactly or approximately. We note that the underlying assumptions for the validity of the

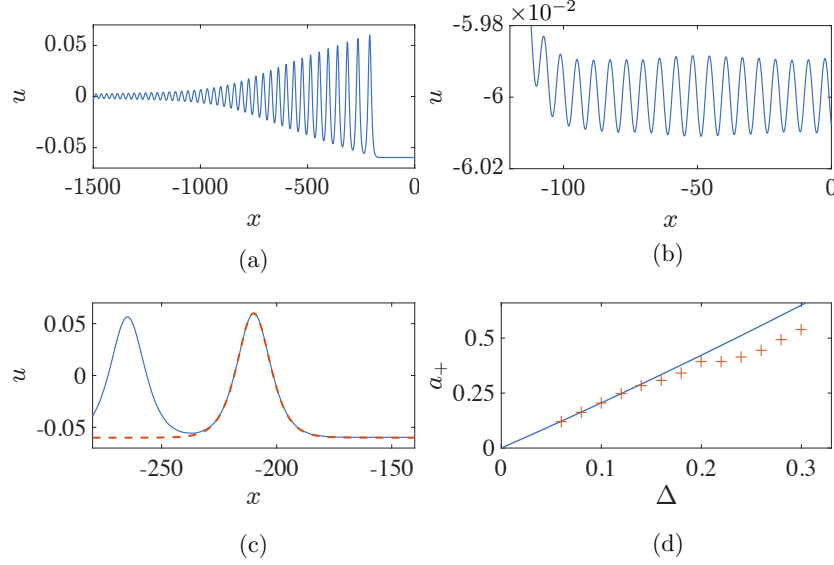


FIGURE 11. Numerically computed Kawahara radiating DSWs in the small jump regime. (a) The solution at  $t \approx 8573$  for jump  $\Delta = 0.06$ . The radiation is not visible due to its small amplitude. (b) Zoomed in view of radiation for RDSW in panel (a). (c) RDSW leading edge from (a) with an overlay of a numerically computed Kawahara solitary wave of the same speed. (d) Comparison of the leading edge amplitude  $a_+$  versus  $\Delta$  incorporating predictions from Kawahara DSW fitting (solid) and extracted values from numerical simulations (pluses).

DSW fitting method require additional considerations, which we do not fully explore here. Rather, we apply the method and compare the results with our numerical simulations.

The RDSW trailing edge wavenumber  $k_-$  is characterized by a simple wave solution of the Whitham modulation equations. This wavenumber can be determined from the solution of the ODE

$$(40) \quad \frac{dk}{d\bar{u}} = \frac{\omega_{\bar{u}}}{\bar{u} - \omega_k} = \frac{1}{3k - 5k^3}, \quad k(-\Delta) = 0,$$

where  $\omega$  is the Kawahara linear dispersion relation (4). The modulation variable  $\bar{u}$  corresponds to the period-mean of the modulated periodic traveling wave and the boundary condition  $k(-\Delta) = 0$  is due to the vanishing of the modulation wavenumber at the RDSW solitary wave edge where  $\bar{u} = -\Delta$ . The ODE (40) can be directly integrated, yielding

$$(41) \quad k(\bar{u})^2 = \frac{3 - \sqrt{9 - 20(\bar{u} + \Delta)}}{5}.$$

The RDSW trailing edge wavenumber is determined by evaluating (41) at the RDSW trailing edge where  $\bar{u} = 0$

$$(42) \quad k_- = k(0) = \left( \frac{3 - \sqrt{9 - 20\Delta}}{5} \right)^{1/2} = \left( \frac{2\Delta}{3} \right)^{1/2} + \frac{5\Delta^{3/2}}{9\sqrt{6}} + \mathcal{O}(\Delta^{5/2}).$$

Reflecting the harmonic wave nature of the trailing edge, its velocity  $s_-$  is then determined by evaluating the Kawahara linear group velocity at the trailing edge

$$(43) \quad s_- = \frac{\partial\omega}{\partial k}(k_-, 0) = -2\Delta + \frac{(3 - \sqrt{9 - 20\Delta})^2}{10} = -2\Delta + \frac{10}{9}\Delta^2 + \mathcal{O}(\Delta^3).$$

There are several ‘‘barriers’’ to the DSW fitting analysis [14]. The first barrier occurs at an extremum of the trailing edge speed as a function of jump height. The minimum of  $s_-(\Delta)$  occurs when  $\Delta = \Delta_i = 27/80 \approx 0.34$ . At this value of  $\Delta$ , the trailing edge wavenumber  $k_- = \sqrt{3/10}$  is precisely the zero dispersion point  $k_i$ . We cannot expect the DSW fitting method to accurately describe RDSWs for  $\Delta > \Delta_i$ . In another

model equation with non-convex dispersion, crossing this barrier led to DSW implosion [25]. Note that the jump height  $\Delta = 9/20$ , above which  $k_-$  becomes complex-valued, exceeds the barrier  $\Delta_1$ .

The second barrier occurs when the hyperbolic Whitham modulation system loses genuine nonlinearity at a linearly degenerate point. This barrier can be identified at the RDSW harmonic wave edge by finding the zero of  $\omega_{k\bar{u}}(\bar{u} - \omega_k) + \omega_{kk}\omega_{\bar{u}}$  [14], which occurs at the jump height  $\Delta = \Delta_1 = 1/4$ . This second barrier occurs at a smaller jump height than the first.

The speed at the DSW leading edge is calculated in a similar manner by first introducing conjugate variables  $\tilde{k}$ , and  $\tilde{\omega}(\tilde{k}, \bar{u}) = -i\omega(i\tilde{k}, \bar{u})$ , where  $\tilde{k}$  acts as an amplitude parameter and  $\tilde{\omega}$  is a ‘‘solitary wave dispersion relation’’. One now solves the ODE

$$(44) \quad \frac{d\tilde{k}}{d\bar{u}} = \frac{\tilde{\omega}_{\bar{u}}}{\bar{u} - \tilde{\omega}_{\tilde{k}}} = -\frac{1}{3\tilde{k} + 5\tilde{k}^3}, \quad \tilde{k}(0) = 0.$$

Integrating and evaluating the conjugate wavenumber at the solitary wave leading edge yields  $\tilde{k}_+^2 = \tilde{k}(-\Delta)^2 = \frac{-3 + \sqrt{9 + 20\Delta}}{5}$ . The DSW leading edge speed  $s_+$  is the conjugate phase velocity evaluated at the leading edge

$$(45) \quad \begin{aligned} s_+ &= \frac{\tilde{\omega}(\tilde{k}_+, -\Delta)}{\tilde{k}_-} = \frac{3}{25} - \frac{1}{5}\Delta - \frac{1}{25}\sqrt{9 + 20\Delta} \\ &= -\frac{1}{3}\Delta + \frac{2}{27}\Delta^2 + \mathcal{O}(\Delta^3). \end{aligned}$$

Utilizing the approximate Kawahara solitary wave amplitude-speed relation (22), we can obtain an estimate for the solitary wave edge amplitude  $a_+$  by equating  $s_+ = c(a_+)$ , yielding

$$(46) \quad a_+ = 2\Delta + \frac{5}{9}\Delta^2 + \mathcal{O}(\Delta^3).$$

We note that all of the small  $\Delta$  asymptotics in eqs. (42), (43), (45), and (46) of the RDSW agree with the results for KdV at leading order in  $\Delta$  [17]. However, the RDSW exhibits an additional, radiative component. Using the RDSW analysis, we can estimate some of the properties of the forward, short-wave radiation. The resonance condition

$$(47) \quad s_+ = \frac{\omega(k_r, -\Delta)}{k_r} = -\Delta - k_r^2 + k_r^4,$$

equates the RDSW leading edge solitary wave speed (47) with the phase speed of linear waves, thus determining the resonant wavenumber  $k_r$

$$(48) \quad \begin{aligned} k_r^2 &= \frac{1}{2} + \frac{1}{10} \left( 37 + 80\Delta - 4\sqrt{9 + 20\Delta} \right)^{1/2} \\ &= 1 + \frac{2}{3}\Delta + \mathcal{O}(\Delta^2). \end{aligned}$$

Because  $k_r$  exceeds the linear dispersion inflection point  $k_i = \sqrt{3/10}$ , resonant radiation corresponds to the positive dispersion regime. We note that this resonant radiation wavenumber agrees with the wavenumber  $\bar{k}$  associated with the TDSW in eq. (35) only at leading order ( $\bar{k} \sim 1 + \frac{1}{4}\Delta$ ,  $0 < \Delta \ll 1$ ).

References [3, 29] provide an asymptotic estimate for the amplitude  $a_r$  of the radiation from an unstable Kawahara solitary wave. Because a lone solitary wave decays due to this linear resonance, the amplitude  $a_r$  was found to be a time-dependent quantity. However, the RDSW leading edge approximate solitary wave is sustained so, using the results of [3, 29], we estimate the *constant* radiation amplitude

$$(49) \quad a_r \sim K \exp\left(-\frac{3\pi}{2\sqrt{\Delta}}\right),$$

where  $K \approx 752.85$  is a numerical constant. Figure 12 compares the numerically extracted RDSW radiation wavenumber  $k_r$  and amplitude  $a_r$  with the predictions of Eqs. (48) and (49). We note that due to fast dispersive propagation to the boundary, it becomes exceedingly difficult to numerically resolve the exponentially small radiation amplitude  $a_r$  for small  $\Delta$ , likely the cause of the discrepancy in Fig. 12(b). This shows, and has been noted previously [15], that a RDSW provides a means to effectively sustain a Kawahara solitary wave—which would otherwise decay due to linear resonance [3]—as part of a DSW. As Fig. 11(d) reveals, the RDSW leading edge amplitude closely follows the prediction in eq. (46) until the jump exceeds about 0.2.

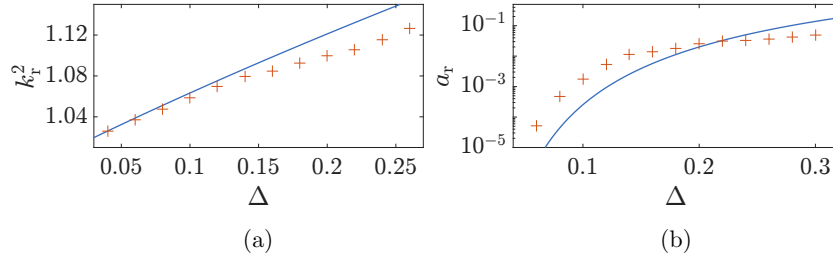


FIGURE 12. Comparison of amplitude of the radiation in the small amplitude RDSW with Analytical prediction from (49) (solid) and extracted values from numerical simulations (pluses).

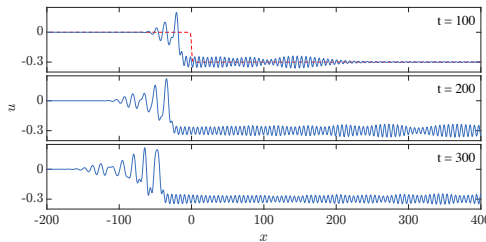


FIGURE 13. Crossover Kawahara DSW dynamics for the intermediate jump value  $\Delta = 0.3$  with  $\sigma = +1$ . Initial data is the dashed curve.

One possible explanation for this could be the apparent loss of genuine nonlinearity in the Whitham equations when  $\Delta > \Delta_1 = 1/4$ . At larger jumps, the RDSW solitary wave edge no longer resembles a Kawahara solitary elevation wave solution, but begins to share qualities with TDSWs. The dynamics begin to lose the rank ordered structure that is characteristic of classical DSWs. We now analyze the intermediate, crossover regime where the DSW structure gradually transitions from RDSWs to TDSWs.

**4.3. Non-convex dispersion with intermediate jumps: the crossover regime.** As the magnitude of the jump initial data increases, the RDSW begins to lose KdV-like characteristics while gaining features of a TDSW. This transition between the RDSW with positive polarity and orientation (small jumps) and the TDSW with negative polarity and orientation (large jumps) occurs gradually as  $\Delta$  is increased in magnitude. The evolution of the GP problem in Fig. 13 is representative of the evolution of step initial data with  $\Delta = 0.3$  and displays significant backward radiation adjacent to a recessed, large amplitude, oscillatory region. The structure of the oscillatory region exhibits slower amplitude decay and more of an amplitude separation from the leading edge than that of the smaller jump depicted in Fig. 11(a). The DSWs for values of  $\Delta$  in this region are qualitatively characterized by this remnant of a small amplitude RDSW with positive polarity and orientation with superimposed small amplitude waves that suggest incoherence. Such incoherence results in wave mixing that eliminates the rank-ordered structure of the RDSWs that occur at smaller jumps. The largest amplitude, elevation wave does not appear to resemble any of the Kawahara solitary waves we have computed in Fig. 4 and waves propagate both ahead of and behind the peak. Just as we identify the leading edge of RDSWs resulting from small jumps with elevation solitary waves in Fig. 4 ( $c > 0$ ) and the TDSW trailing edge for large jumps with non-monotonic elevation solitary waves ( $c < -1/4$ ), we interpret the intermediate jump transition region as corresponding to the solitary wave “band gap” for  $-1/4 < c < 0$  in Fig. 4. For velocities in the band gap, solitary waves do not exist. However, we can compute periodic traveling waves in this region so a modulation description may be possible, but we do not pursue this further here. Rather, we seek to identify when the backward radiation on  $u = 0$  emanating from the transition to  $u = -\Delta$  ceases, signifying the onset of the steady TDSW.

If these backward radiating waves were, in fact, linear then they could persist whenever the linear phase velocity on zero background coincides with the edge speed, otherwise we expect a TDSW. The linear phase velocity  $v_{ph} = \omega(k, 0)/k = -k^2 + k^4$  attains a minimum value of  $-1/4$  precisely when the phase and group velocities coincide  $k = 1/\sqrt{2}$  and when the non-monotonic Kawahara solitary waves appear (cf. Fig. 4).

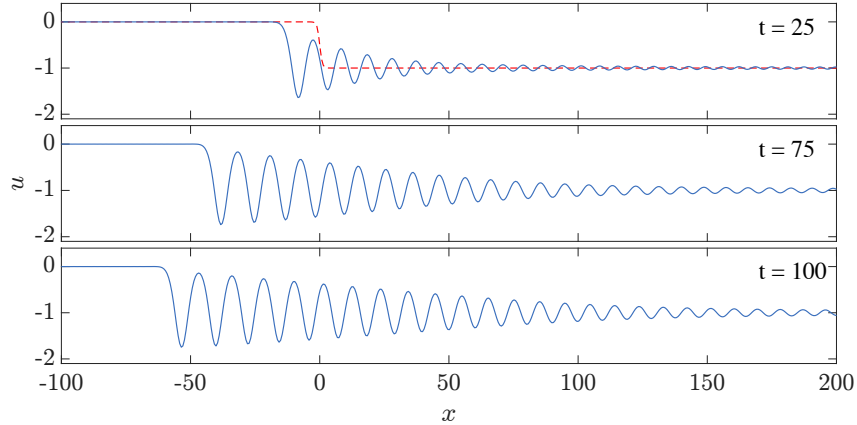


FIGURE 14. Development of a classical Kawahara DSW with initial jump  $\Delta = 1$  and convex dispersion  $\sigma = -1$ . Approximate initial data is shown in the top figure with the dashed curve.

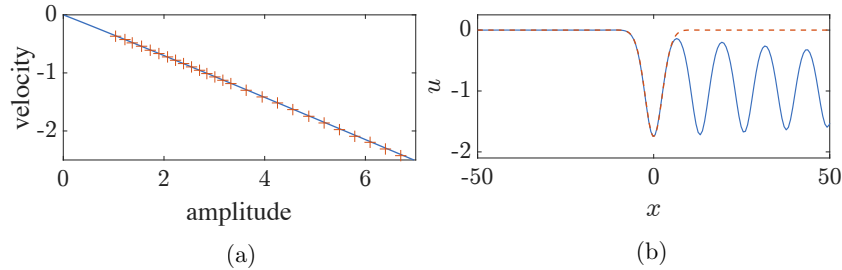


FIGURE 15. Comparison of DSW leading edge properties to Kawahara solitary waves. (a) Speed-amplitude relation of Kawahara solitary wave (solid) and DSW trailing edge (pluses) for  $\sigma = +1$ . (b) Overlay of numerically computed solitary wave with coincident velocity with the DSW trailing edge for  $\Delta = 1$ .

Equating the minimum of  $v_{\text{ph}}$  to the TDSW leading order gRH (34),  $c = -\Delta/2$  gives the critical jump height  $\Delta_{\text{cr}} \sim \frac{1}{2}$ , above which linear waves cannot propagate behind the TDSW. However, the numerical simulations show that waves continue to propagate backward even when  $\Delta = 1/2$ . Our numerical simulations have shown that this phenomenon persists up to jumps of  $\Delta \approx 0.6$ . Although close to the theoretical prediction, we argue that the true threshold criterion is the existence of the TDSW traveling wave. We found in Section 4.1.1 that we could no longer compute TDSWs for  $\Delta$  below 0.58, very close to the observed transition to TDSWs at  $\Delta = 0.6$ . Therefore, the TDSW is a *threshold* phenomenon, only existing for  $\Delta > \Delta_{\text{cr}}$ . For  $\Delta < \Delta_{\text{cr}}$ , either perturbed, classical DSWs are generated as in Section 4.2 (when  $\Delta \lesssim 0.2$  from Fig. 11(d)) or a crossover, oscillatory state lacking a well-defined solitary wave edge.

**4.4. Convex dispersion.** In the case where the sign of the third order term is negative ( $\sigma = -1$ ), the Kawahara dispersion relation (4) is a purely convex function of  $k$ . These are “convex dispersive hydrodynamics” so we expect KdV-like DSWs. For completeness, we briefly analyze this case.

The numerical simulation in Fig. 14 depicts the temporal evolution of step initial data (23) for eq. (3). This figure portrays the temporal development of a DSW that is qualitatively similar to the classical KdV DSW. The addition of the fifth order term in eq. (3) serves as a perturbation to the KdV equation that, in contrast to the non-convex case  $\sigma = +1$ , does not qualitatively change the dynamics. The DSW trailing edge behaves like a solitary wave solution of the Kawahara equation as shown by Fig. 15(a) where the DSW trailing edge speed-amplitude relation, extracted from multiple simulations, is compared to the solitary wave amplitude speed relation from Fig. 3. A Kawahara solitary wave of velocity given by the trailing edge is superimposed on the DSW trailing edge in Fig. 15(b).

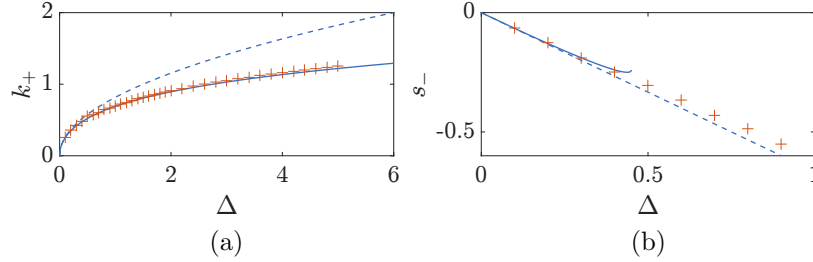


FIGURE 16. Kawahara DSW trailing edge wavenumber (a) and DSW leading edge speed (b) for varying jump height. Comparison between Whitham theory predictions for the Kawahara equation (solid), Whitham theory for the KdV equation (dashed) and numerical simulation (pluses).

We now implement the DSW fitting method [12] (see also [14]). The implementation is essentially the same as that of Section 4.2 but we now use the dispersion relation (4) and approximate solitary wave amplitude-speed relation (22) both with  $\sigma = -1$ . We omit the details. The macroscopic DSW harmonic leading edge properties are the characteristic wavenumber

$$(50) \quad k_+ = \left( \frac{-3 + \sqrt{9 + 20\Delta}}{5} \right)^{1/2} = \left( \frac{2\Delta}{3} \right)^{1/2} - \frac{5\Delta^{3/2}}{9\sqrt{6}} + \mathcal{O}(\Delta^{5/2}),$$

and speed

$$(51) \quad s_+ = \frac{9}{5} + 3\Delta - \frac{3}{5}\sqrt{9 + 20\Delta} = \Delta + \frac{10}{9}\Delta^2 + \mathcal{O}(\Delta^3).$$

Figure 16(a) shows the DSW harmonic edge wavenumber  $k_+$  versus jump height. DSW fitting theory provides an excellent approximation of the trailing edge wavenumber, extracted from our numerical simulations. In particular, DSW fitting correctly captures the reduction of the trailing edge wavenumber relative to the leading order KdV result  $k_+ = \sqrt{2\Delta/3}$ . We see that higher order dispersion has a significant quantitative effect on the properties of the harmonic wave edge.

The macroscopic properties of the DSW solitary wave trailing edge include the velocity

$$(52) \quad s_- = \frac{3}{25} - \frac{4}{5}\Delta - \frac{1}{25}\sqrt{9 - 20\Delta} = -\frac{2}{3}\Delta + \frac{2}{27}\Delta^2 + \mathcal{O}(\Delta^3),$$

and the amplitude

$$(53) \quad a_- = 2\Delta - \frac{5}{9}\Delta^2 + \mathcal{O}(\Delta^3),$$

approximated by using eq. (22) and equating  $s_- = c(a_-)$ . Although the trailing edge velocity is only defined for  $0 < \Delta < 9/20$ , the small  $\Delta$  asymptotics agree with the KdV velocity (and amplitude  $a_+$ ) to leading order [17]. The next order correction shows that the Kawahara DSW solitary wave edge velocity is above the corresponding KdV DSW velocity, which agrees with the numerical simulations shown in Fig. 16(b) for  $\Delta$  below the critical value  $9/20$ . The DSW fitting method fails for  $\Delta > 9/20$ , even though numerical computations show a clear trend.

## 5. DISCUSSION/CONCLUSION

The Kawahara equation is a universal asymptotic model of weakly nonlinear, dispersive hydrodynamics with higher order dispersion. The classification of the Gurevich-Pitaevskii initial step problem carried out here reveals classical, KdV-like DSWs when the dispersion is convex and three distinct regimes for non-convex dispersion. These three regimes represent an intrinsic mechanism for the transition from convex to non-convex dispersive hydrodynamics. An example from shallow water waves (recall Section 2.1) illuminates this transition.

When gravity dominates surface tension effects, the Bond number  $B$  is small so that higher order dispersive effects continue to yield negative dispersion curvature for all but very short wavelengths (recall eq. (16)). DSWs in this regime are therefore KdV-like, satisfying eq. (1) with  $\sigma = +1$ , with positive orientation and

polarity as in Fig. 1(b). For  $B$  less than but close to  $1/3$ , where surface tension and gravity start to balance, the non-convexity of the dispersion relation manifests in the Kawahara equation (3) with  $\sigma = +1$ . Small jumps still yield KdV-like DSWs with positive orientation and polarity but now they are accompanied by a resonance and small amplitude forward radiation. They are RDSWs. As the jump height is further increased, the forward radiation gets stronger at the expense of backward wave propagation until a critical jump height is reached. Above this threshold, a TDSW with negative orientation and polarity is generated, exhibiting a steady traveling wave structure at the trailing edge. Thus, the crossover from positive to negative DSW polarity and orientation manifests as an intrinsic feature of the Kawahara equation as the jump height is increased. For  $B > 1/3$ ,  $\sigma = -1$  and the DSWs are all KdV-like with negative polarity and orientation. Because the Bond number is inversely proportional to fluid depth, we expect to see these non-convex features for sufficiently shallow flows.

Higher order dispersive effects can play an important role in nonlinear fiber optics as demonstrated in [6–9, 26]. The Kawahara equation is a simpler, scalar, unidirectional model in which to interpret the dynamics of these works (cf. Section 2.2). In particular, the authors in [6] observed coherent structures consistent with RDSWs and TDSWs described in detail here. Solitary wave and DSW resonances modeled by a third order NLS equation were observed experimentally in [9]. This motivates further analysis of higher order NLS models. Can TDSW traveling wave solutions of the bidirectional NLS equation with third order dispersion be obtained? Also, the implications of these coherent structures for physical applications warrants further exploration.

The TDSW is a non-classical DSW in the sense that it is not KdV-like, rather it satisfies a generalized Rankine-Hugoniot relation resulting from the far-field behavior of a constant in one direction and a periodic traveling wave in the other. The TDSW rapidly approaches a traveling wave solution of the Kawahara equation satisfying these far-field conditions, consisting of a coherent combination of a uniform wavetrain connected to the constant value through a partial, non-monotonic solitary wave. The fact that the Kawahara traveling wave ODE is fourth order enables this solution. It is natural to conjecture that the TDSW consists of a periodic orbit solution to the traveling wave ODE that is heteroclinic to an equilibrium, generalizing homoclinic and heteroclinic solutions studied previously [18]. An open question is the rigorous existence of a traveling wave solution of the Kawahara equation exhibiting this structure. Nonuniformity in the leading edge of the TDSW corresponds to a forward propagating wavepacket moving with the group velocity for a distinct wavenumber, approximately that of the periodic orbit. The uniform wavetrain acts as a channel for the effective dissipation of energy. Interestingly, the TDSW only exists for sufficiently large jumps  $\Delta \gtrsim 0.60$ , below which waves radiate forward and backward from the sharp transition region due to the Kawahara solitary wave band gap.

The generalized Rankine-Hugoniot condition is a kind of nonlinear resonance condition in the sense that the trailing edge solitary wave velocity coincides with the adjacent periodic traveling wave velocity. Such a condition has been assumed previously [6, 15] but here we show that it is inherent in the generation of a traveling wave structure within the TDSW.

Although a non-convex dispersion can give rise to TDSWs above threshold, it is not necessary. Another model equation, the conduit equation, also with non-convex dispersion, does not exhibit such solutions [25]. But that model, a Benjamin-Bona-Mahony type equation [4] with nonlinear dispersion, does display non-classical DSW dynamics at the DSW harmonic wave edge. Likely, the principle reason that TDSWs do not occur is the lack of a linear resonance at the DSW solitary wave edge.

A unique feature of the TDSW is its triple personality. On the one hand, it is similar to a dissipative shock wave in that it satisfies a generalized Rankine-Hugoniot condition and exhibits a steady character when viewed near the shock front. On the other hand, the TDSW is similar to a classical DSW, exhibiting two distinct limits: a small amplitude, harmonic edge moving with the group velocity and a large amplitude solitary wave edge moving with the phase velocity. But the TDSW is distinct in that the transition from a periodic wave to a solitary wave occurs almost instantaneously, setting it apart from DSWs in convex dispersive hydrodynamics and shock waves in dissipative hydrodynamics.

#### ACKNOWLEDGMENTS

The authors are grateful to James Meiss for insightful discussions.

## REFERENCES

- [1] V. ACHILLEOS, D. J. FRANTZESKAKIS, P. G. KEVREKIDIS, AND D. E. PELINOVSKY, *Matter-wave bright solitons in spin-orbit coupled Bose-Einstein condensates*, Physical Review Letters, 110 (2013).
- [2] I. BAKHOLDIN, *Non-dissipative discontinuities in continuum mechanics*, Fizmatlit, Moscow, 2004. in Russian.
- [3] E. BENOLOV, R. GRIMSHAW, AND E. KUZNETSOVA, *The generation of radiating waves in a singularly-perturbed Korteweg-de Vries equation*, Physica D, 69 (1993), pp. 270–278.
- [4] T. B. BENJAMIN, J. L. BONA, AND J. J. MAHONY, *Model equations for long waves in nonlinear dispersive systems*, Philos. T R Soc. S-A, 272 (1972), pp. 47–78.
- [5] D. C. CALVO, T.-S. YANG, AND T. AKYLAS, *On the stability of solitary waves with decaying oscillatory tails*, Proc. R. Soc. A.
- [6] M. CONFORTI, F. BARONIO, AND S. TRILLO, *Resonant radiation shed by dispersive shock waves*, Phys. Rev. A, 89 (2014), 013807.
- [7] M. CONFORTI AND T. S., *Dispersive wave emission from wave breaking*, Opt. Lett., 38 (2013), pp. 3815–3818.
- [8] M. CONFORTI AND T. S., *Radiative effects driven by shock waves in cavity-less four-wave mixing combs*, Opt. Lett, 39 (2014), pp. 5760–5763.
- [9] M. CONFORTI, T. S., M. A., AND K. A., *Parametric excitation of multiple resonant radiations from localized wavepackets*, Sci. Rep., 5 (2015), pp. 1–5.
- [10] F. DIAS AND P. MILEWSKI, *On the fully-nonlinear shallow-water generalized Serre equations*, Phys. Lett. A, 374 (2010), pp. 1049–1053.
- [11] B. DUBROVIN, T. GRAVA, AND C. KLEIN, *Numerical study of breakup in generalized Korteweg-de Vries and Kawahara equations*, SIAM J. Appl. Math, 71 (2011), p. 983.
- [12] G. EL, *Resolution of a shock in hyperbolic systems modified by weak dispersion*, Chaos, 15 (2005), p. 7103.
- [13] G. EL, M. HOEFER, AND M. SHEARER, *Dispersive and diffusive-dispersive shock waves for nonconvex conservation laws*, SIAM Rev., accepted, (2016), arXiv:1501.01681 [nlin.PS].
- [14] G. A. EL AND M. A. HOEFER, *Dispersive shock waves and modulation theory*, Physica D, (2016), doi:10.1016/j.physd.2016.04.006.
- [15] G. A. EL AND N. F. SMYTH, *Radiating dispersive shock waves in non-local optical media*, Proc. R. Soc. A, 472 (2016), p. 2187.
- [16] R. GRIMSHAW, B. MALOMED, AND E. BENOLOV, *Solitary waves with damped oscillatory tails: an analysis of the fifth-order Korteweg-de Vries equation*, Physica D: Nonlinear Phenomena, 77 (1994), pp. 473–485.
- [17] A. V. GUREVICH AND L. P. PITAEVSKII, *Nonstationary structure of a collisionless shock wave*, Sov. Phys. JETP, 38 (1974), pp. 291–297.
- [18] M. HARAGUS AND G. IOOSS, *Local bifurcations, center manifolds, and normal forms in infinite-dimensional dynamical systems*, Springer London, London, 2011.
- [19] J. K. HUNTER AND J. SCHEURLE, *Existence of perturbed solitary wave solutions to a model equation for water waves*, Physica D, 32 (1988), pp. 253–268.
- [20] A. T. ILICHEV AND V. Y. TOMASHPOLSKII, *Soliton-like structures on a liquid surface under an ice cover*, Theor. Math. Phys., 182 (2015), pp. 231–245.
- [21] R. S. JOHNSON, *A modern introduction to the mathematical theory of water waves*, Cambridge University Press, Cambridge, 1997.
- [22] T. KAWAHARA, *Oscillatory solitary waves in dispersive media*, J. Phys. Soc. Jpn, 33 (1972), pp. 260–264.
- [23] Y.-J. LIN, R. L. COMPTON, K. JIMNEZ-GARCA, J. V. PORTO, AND I. B. SPIELMAN, *Synthetic magnetic fields for ultracold neutral atoms*, Nature, 462 (2009), pp. 628–632.
- [24] Y.-J. LIN, K. JIMNEZ-GARCA, AND I. B. SPIELMAN, *Spin-orbit-coupled Bose-Einstein condensates*, Nature, 471 (2011), pp. 83–86.
- [25] N. K. LOWMAN AND M. A. HOEFER, *Dispersive shock waves in viscously deformable media*, J. Fluid Mech., 718 (2013), pp. 524–557.
- [26] S. MALAGUTI, M. CONFORTI, AND S. TRILLO, *Dispersive radiation induced by shock waves in passive resonators*, Opt. Lett., 39 (2014), pp. 5626–5629.
- [27] A. MARCHENKO, *Long waves in shallow liquid under ice cover*, J. Appl. Math, 52 (1988), pp. 180–183.
- [28] Y. MATSUNO, *Hamiltonian formulation of the extended Green-Naghdi equations*, Physica D, 301 (2015), pp. 1–7.
- [29] Y. POMEAU, A. RAMANI, AND B. GRAMMATICOS, *Structural stability of the Korteweg-de Vries solitons under a singular perturbation*, Physica D, 31 (1988), pp. 127–134.
- [30] Y. TAN, J. YANG, AND D. E. PELINOVSKY, *Semi-stability of embedded solitons in the general fifth-order KdV equation*, Wave Motion, 36 (2002), pp. 241–255.
- [31] G. B. WHITHAM, *Linear and Nonlinear Waves*, vol. 42, John Wiley & Sons, 2011.
- [32] J. YANG, *Newton-conjugate-gradient methods for solitary wave computations*, J. Comput. Phys., 228 (2009), pp. 7007–7024.